J. Fluid Mech. (1993), *vol.* 246, *pp.* 443–464

Spin-up from rest of a mixture: numerical simulation and asymptotic theory

By GUSTAV AMBERG[1] AND MARIUS UNGARISH[2]†

[1] Department of Hydromechanics, Royal Institute of Technology, S-100 44 Stockholm, Sweden

[2] Department of Computer Science, Technion-Israel Institute of Technology, Haifa 32000, Israel

(Received 9 January 1992 and in revised form 16 June 1992)

Spin-up from rest of a separating fluid–particle mixture is studied. A cylindrical container, filled with a stationary mixture of initially uniform particle volume fraction, is instantaneously set into rapid rotation. The viscous forces on the walls introduce a secondary Ekman-layer circulation which causes the fluid motion to gradually approach a state of solid-body rotation. While the mixture acquires angular momentum, separation starts under the action of the local centrifugal effects: the dispersed particles – assumed here to be lighter than the fluid – tend to concentrate around the centre, leaving behind a peculiarly shaped domain of pure fluid. This process is simulated by a finite difference version of the 'mixture model' equations. The numerical results are in good agreement with previous asymptotical predictions but also illuminate some aspects of the flow field that have been covered by the analytical approach.

1. Introduction

Spin-up from rest concerns the transient motion of an initially stationary fluid which is subsequently exposed to the action of a spinning solid boundary and eventually acquires a steady state of prevailing angular velocity; in idealized circumstances, all the solid boundaries in contact with the fluid rotate at the same angular velocity $\boldsymbol{\Omega}^*$ and the final velocity of the fluid is that of 'solid-body rotation', $\boldsymbol{\Omega}^* \times \boldsymbol{r}^*$. The transient velocity field is usually governed by a secondary convective motion sustained by quasi-steady thin viscous layers and practically completed on a very special 'spin-up timescale', which is roughly the geometric mean between the period of revolution and the conventional viscous diffusion time interval.

Spin-up from rest is evidently an intrinsic stage of centrifugal processing of suspensions. The fact that considerable separation may take place before the conventional $\boldsymbol{\Omega}^* \times (\boldsymbol{\Omega}^* \times \boldsymbol{r}^*)$ field is established in the mixture provides the already fascinating spin-up process with additional physical features and formulation challenges. The investigation of this problem therefore serves several purposes: gaining physical insight, assessing the ability of the averaged continuum formulation to treat complicated non-intuitive flow fields, testing numerical solvers and providing the background for a thorough comparison with experiments.

The present paper uses a numerical finite-difference solution of the 'mixture model' to throw additional light on the spin-up from rest and separation process of a suspension of light particles in a cylindrical container.

† To whom correspondence should be addressed.

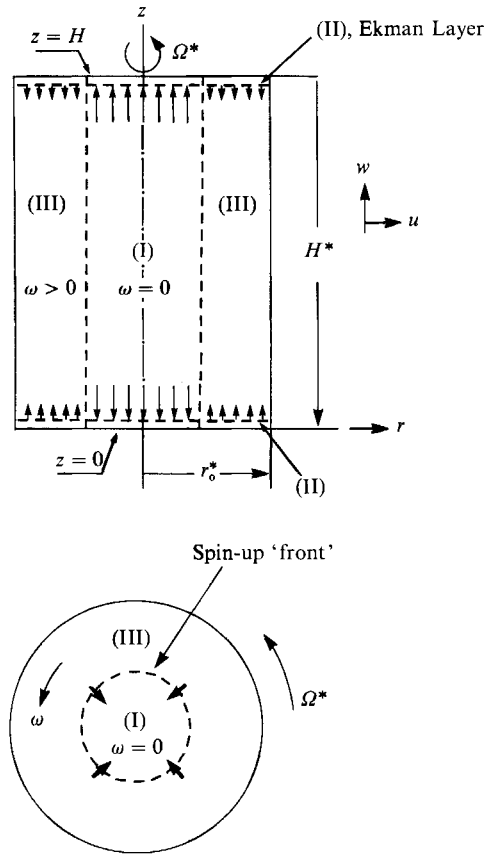

FIGURE 1. Geometry and schematic motion of single-phase spin-up.

The spin-up from rest in a cylindrical container, instantaneously set into rapid rotation Ω^* around its axis of symmetry z is a fundamental problem. The flow field of a homogeneous (single-phase) fluid has been studied analytically by Wedemeyer (1964), Venezian (1970) and others. A corresponding numerical simulation, including comparison with the above-mentioned analytical results and experiments, has been presented by Hyun *et al.* (1983). The main features are as follows, see figure 1: an inwardly moving cylindrical 'spin-up front' separates between the non-rotating inner core I and the partly spun-up region III; the quasi-steady very thin Ekman layers on the top and bottom caps, referred to as region II, continuously extract fluid from sector I and feed it into domain III; the process is effectively completed when all the non-rotating fluid has been flushed into region III, and the typical spin-up timescale is $\tau^*_{su} = [(E^{\frac{1}{2}}/H)\,\Omega^*]^{-1}$.

Here $E = \nu_0^*/\Omega^* r_o^2$ is the Ekman number, usually a very small parameter; $H = H^*/r_o^*$ is the aspect ratio – or dimensionless height – of the container; ν_0^* is the kinematic viscosity of the fluid; Ω^*, r_o^* and H^* are the angular velocity, outer radius and height of the container, respectively (the asterisk designates dimensional variables).

The flow field of a non-colloidal monodispersed suspension (two-phase) fluid has been investigated by Ungarish (1990, 1991). The dispersed particles (or droplets) of radius a^* and density ρ_D^* are initially well mixed in the embedding fluid whose

density is ρ_C^*, so the initial volume fraction (or concentration) is $\epsilon(0)$ throughout the container. The additional basic parameters are: the density difference, $\alpha = (\rho_D^* - \rho_C^*)/\rho_C^*$; the (modified) particle Taylor number $\beta = \frac{2}{9}a^{*2}\Omega^*/\nu_0^*$; and the initial volume fraction $\epsilon(0)$. From the physical standpoint, a new effect is introduced, namely, the separation of the suspension due to centrifugal buoyancy, associated with the timescale $\tau_{scp}^* = (|\alpha|\beta\Omega^*)^{-1}$. The ratio $\lambda = \tau_{sep}^*/\tau_{su}^*$ is bound to play a significant role in the combination of spin-up and separation.

The governing equations of motion for the averaged variables, which are usually of concern in flow of suspensions, can be formulated as the 'mixture model' or as the 'two-fluid model'. The former can be regarded as an extension of the more familiar single-phase case (global continuity and momentum balances) supplemented by one equation for the volume fraction of the dispersed component, ϵ. The latter model is more sophisticated, containing continuity and momentum balances for both the 'continuous' and 'dispersed' components ('phases'), with interaction terms. The asymptotic approach to the problem of spin-up from rest, which will be briefly reviewed in §3, is based on the mixture model equations. Qualitative support to the analysis was given by a numerical solution of the two-fluid formulation for the heavier suspended particles case, $\alpha > 0$, mentioned by Ungarish (1990). Obviously, a quantitative comparison could become awkward and inconclusive because in such complex flow fields a significant – but unknown – portion of the discrepancies can be attributed to intrinsic differences between the models.

The present work attempts to extend the previous results in several respects. Numerical solutions for the flow field with lighter suspended particles, $\alpha < 0$, are obtained and discussed. This configuration is particularly challenging because of the moving curved interface (kinematic shock) between the central mixture bulk and the peripheral pure fluid region, but its numerical corroboration was not available. The numerical scheme is applied to the mixture model equations, with two purposes in mind: (*a*) to provide unequivocal results for comparison with the approximate theory (based on the same equations); (*b*) to verify that the numerical solution of this model for complicated flow problems can be achieved by non-sophisticated extensions of single-phase schemes within moderate programming efforts. In general, the favourable comparison, and the interpretation of the slight discrepancies, between the new numerical and previous analytical data yield useful information on and insight into the flow concerned and on the computational approach.

2. Formulation

The fundamental problem of spin-up in a straight circular cylinder is considered. The height of the cylinder is H^*, its radius r_o^*, see figure 1. (Asterisks are used throughout to denote dimensional quantities.) At time $t^* = 0$, the cylinder is completely filled with a mixture of fluid and particles of homogeneous volume fraction $\epsilon(0)$. Initially the mixture is stationary. The container is, at $t^* = 0$, brought impulsively to a constant angular velocity Ω^* around its axis of symmetry. The mixture will gradually approach a state of solid-body rotation and separation will be induced by the centrifugal force, as soon as the mixture has acquired any appreciable azimuthal velocity. Here the detailed treatment will be devoted to particles that are lighter than the fluid, which consequently will settle inward, but the formulation is for the general case.

In formulating the equations that govern this process, we shall employ variables that are made non-dimensional by using the following scales: outer radius r_o^* for

length, $1/\Omega^*$ for time, $r_0^*\Omega^*$ for velocity, ρ_C^* for density, and $\rho_C^*(\Omega^* r_0^*)^2$ for pressure. The subscripts C and D denote the continuous and the dispersed (particles) phases, respectively.

The four basic non-dimensional numbers that govern the process are

$$E = \frac{\nu_0^*}{\Omega^* r_0^{*2}}; \quad \alpha = \frac{\rho_D^* - \rho_C^*}{\rho_C^*}; \quad \beta = \frac{2}{9}\frac{a^{*2}\Omega^*}{\nu_0^*}; \quad H = \frac{H^*}{r_0^*}. \tag{1}$$

Here E is the Ekman number, which indicates the magnitude of viscous force compared to Coriolis force in the main flow region; α denotes the relative density difference; β is the Taylor number which represents the ratio of Coriolis to viscous drag on a dispersed particle; H is the non-dimensional height, i.e. the aspect ratio, of the container. In the cases of interest here, E and β are small, meaning that the bulk flow is dominated by rotational effects, while the flow around a dispersed particle is dominated by viscous terms.

The momentum equation for the fluid–particle mixture is formulated in the standard way (Ishii 1975). Using an inertial frame of reference, and the present non-dimensional variables, it is

$$(1+\epsilon\alpha)\left(\frac{\partial \boldsymbol{v}}{\partial t} + \boldsymbol{v}\cdot\nabla\boldsymbol{v}\right) = -\nabla p + E\nabla\cdot(\mu(\epsilon)[\nabla\boldsymbol{v} + (\nabla\boldsymbol{v})^{\mathrm{T}} - \tfrac{2}{3}\boldsymbol{I}\nabla\cdot\boldsymbol{v}]) - \nabla\cdot\epsilon(1-\epsilon)\frac{1+\alpha}{1+\alpha\epsilon}\boldsymbol{v}_{\mathrm{R}}\boldsymbol{v}_{\mathrm{R}}. \tag{2}$$

Both particles and fluid are assumed incompressible, so total mass conservation requires that

$$\nabla\cdot\boldsymbol{j} = 0. \tag{3}$$

The conservation of suspended particles is described by

$$\frac{\partial \epsilon}{\partial t} + \nabla\cdot(\epsilon\boldsymbol{v}_{\mathrm{D}}) = 0. \tag{4}$$

In these equations ϵ denotes the volume fraction of particles at a given point, $\boldsymbol{v}$ and $\boldsymbol{j}$ are the averaged mass velocity and the volume velocity (flux) respectively. Let $\boldsymbol{v}_{\mathrm{D}}$ and $\boldsymbol{v}_{\mathrm{C}}$ denote the averaged velocities of particles and fluid, respectively, and $\boldsymbol{v}_{\mathrm{R}}$ is the relative velocity between the phases. These satisfy the following kinematic relationships:

$$\boldsymbol{v} = \frac{(1+\alpha)\epsilon\boldsymbol{v}_{\mathrm{D}} + (1-\epsilon)\boldsymbol{v}_{\mathrm{C}}}{1+\alpha\epsilon}, \quad \boldsymbol{j} = \epsilon\boldsymbol{v}_{\mathrm{D}} + (1-\epsilon)\boldsymbol{v}_{\mathrm{C}}, \tag{5}$$

$$\boldsymbol{v}_{\mathrm{D}} = \boldsymbol{j} + (1-\epsilon)\boldsymbol{v}_{\mathrm{R}}, \quad \boldsymbol{j} = \boldsymbol{v} - \alpha\epsilon\frac{(1-\epsilon)}{1+\alpha\epsilon}\boldsymbol{v}_{\mathrm{R}}. \tag{6}$$

It is postulated that the relative motion between the phases is governed by a local balance between centrifugal buoyancy and Stokesian drag which yields

$$\boldsymbol{v}_{\mathrm{R}} = \boldsymbol{v}_{\mathrm{D}} - \boldsymbol{v}_{\mathrm{C}} = -\alpha\beta\frac{1-\epsilon}{\mu(\epsilon)}\left(\frac{\partial \boldsymbol{v}}{\partial t} + \boldsymbol{v}\cdot\nabla\boldsymbol{v}\right). \tag{7}$$

The function $\mu(\epsilon)$ correlates the effective viscosity with that of the pure embedding fluid and the volume fraction (Ishii & Zuber 1979):

$$\mu(\epsilon) = \frac{\mu_{\mathrm{eff}}^*}{\mu_0^*} = \left(1 - \frac{\epsilon}{\epsilon_{\mathrm{M}}}\right)^{-2.5\epsilon_{\mathrm{M}}}; \tag{8}$$

ϵ_M is the maximum volume fraction in the sediment, which is taken to be 0.62. Note that $v_R \to 0$ as $\epsilon \to \epsilon_M$.

The initial conditions describe the mixture at rest with a given homogeneous volume fraction:

$$v = 0; \quad \epsilon = \epsilon(0) \quad \text{at} \quad t = 0. \tag{9}$$

Boundary conditions are prescribed as follows: on the wall the velocity of the mixture equals with that of the container, and the normal flux of particles vanishes,

$$v = \hat{z} \times r; \quad n \cdot (\epsilon v_D) = 0 \quad \text{at container walls.} \tag{10}$$

Here $\hat{z}$ is the unit vector parallel to the axis of rotation, and n is the normal to the container wall. In the present problem ϵv_R on the walls will be zero, hence the foregoing conditions also imply $n \cdot j = 0$ on the boundary by virtue of (6). It is emphasized that in the equations of motion and boundary conditions no explicit distinction is made between regions of pure fluid ($\epsilon = 0$), sediment ($\epsilon \to \epsilon_M$) and mixture.

3. Some asymptotic results

Analytical solutions to the foregoing formulation in the asymptotic range of small $E, \beta, \epsilon|\alpha|$ have been developed by Ungarish (1990, 1991). For completeness and convenient reference some pertinent results are outlined below.

The viscous regions on the endplates $z = 0, H$, referred to as Ekman layers, become a dominant factor of concern. From homogeneous (single-phase) fluid studies a great deal of useful information about the layers is gained; in particular, it is known that their representative thickness is $\delta_E^* = (\nu_0^*/\Omega^*)^{\frac{1}{2}}$. It can be argued that this knowledge carries over to rotating mixtures, provided that the radius of the dispersed particle, a^*, is much smaller than δ_E^*. To employ this advantage the analysis is restricted to $\beta \ll 1$ since the definition of the Taylor number in (1) can be reformulated as $\beta = \frac{2}{9}(a^*/\delta_E^*)^2$.

The fundamental configuration is sketched in figure 1. It is assumed that the Ekman layers are very thin, a condition expressed by

$$E^{\frac{1}{2}} = (\delta_E^*/r_0^*) = (\nu_0^* \Omega^*/r_0^2)^{\frac{1}{2}} \ll 1;$$

the aspect ratio H is considered of order unity. Consequently, the flow field in the cylinder is envisaged as a combination of Ekman layers on $z = 0, H$ and an interior, mostly inviscid 'core' in the region $0^+ \leqslant z \leqslant H^-, 0 \leqslant r \leqslant 1$. Moreover, the Ekman layers are considered quasi-steady because they show up and adjust during about one revolution of the vessel, while spin-up and separation are much slower.

It is convenient to introduce the effective Ekman number,

$$\mathscr{E} = \mathscr{M}^2 E \tag{11}$$

where

$$\mathscr{M} = (\mu[\epsilon(0)])^{\frac{1}{3}} \tag{12}$$

and the spin-up reduced time coordinate,

$$\tau = t^*/\tau_{su}^* = t(E^{\frac{1}{2}}/H); \tag{13}$$

thus τ is of order unity in the process under investigation.

During spin-up, the angular velocity of the endplates is larger than that of the core, therefore a volume transport $O(\mathscr{E}^{\frac{1}{2}})$ from the centre towards the periphery takes

	Region I $0 \leqslant r^2 \leqslant A$	Region III $A \leqslant r^2 \leqslant 1$
$\mathscr{E}^{-\frac{1}{2}}Hu$	$-r$	$[A/(1-A)][r-1/r]$
ω	0	$[1/(1-A)][1-A/r^2]$
$\mathscr{E}^{-\frac{1}{2}}w$	$[2z/H-1]$	$-[A/(1-A)][2z/H-1]$

TABLE 1. Velocity field in the core $0^+ < z < H^-$. $A = \mathrm{e}^{-2\mathscr{M}\tau}$

place in the Ekman layers. To match this, the variables in the 'core' are of the following orders of magnitude: $\omega = v/r \sim 1$; $u, u_{\mathrm{R}}, w \sim \mathscr{E}^{\frac{1}{2}}$; $v_{\mathrm{R}}, w_{\mathrm{R}} \sim \mathscr{E}^{\frac{2}{3}}$. Under the assumption that $|\alpha|\,\epsilon \leqslant O(\mathscr{E}^{\frac{1}{2}})$, then to leading order in $\mathscr{E}^{\frac{1}{2}}$, the following conclusions can be drawn.

(i) In the 'core' region the pressure p, angular velocity ω and radial velocities u, u_{R} are z-independent, i.e. functions of r and τ only. The axial velocity varies linearly with z.

(ii) The spin-up is decoupled from separation, i.e. the velocity field is governed by the shear interactions on the boundaries (via the Ekman layers). The migration of the heavier component of the mixture to the periphery has negligible influence on the momentum balances.

Hence, to leading order, the velocity field is essentially provided by Wedemeyer's (1964) single-phase approximation: the spin-up 'front' $r = \mathrm{e}^{-\mathscr{M}\tau}$ divides the non-rotating region I and the partially rotating region III, see figure 1, with the appropriate velocities given in table 1.

In this mixture velocity field, the relative velocity (7) is, again to leading order,

$$\boldsymbol{v}_{\mathrm{R}} = \frac{\mathscr{E}^{\frac{1}{2}}}{H}\frac{\alpha}{|\alpha|}\frac{1}{\lambda\mathscr{M}}\frac{1-\epsilon}{\mu(\epsilon)}r\omega^2(r,\tau)\,\hat{\boldsymbol{r}}; \tag{14}$$

and the conservation of the dispersed phase (4) takes the form

$$\frac{1}{\mathscr{M}}\frac{\partial\epsilon}{\partial\tau}+\left[(\mathscr{E}^{-\frac{1}{2}}Hu)+\frac{\alpha}{|\alpha|}\frac{1}{\lambda\mathscr{M}}\frac{\mathrm{d}\Phi(\epsilon)}{\mathrm{d}\epsilon}\omega^2 r\right]\frac{\partial\epsilon}{\partial r}+(\mathscr{E}^{-\frac{1}{2}}w)H\frac{\partial\epsilon}{\partial z}=-\frac{\alpha}{|\alpha|}\Phi(\epsilon)\frac{1}{\lambda\mathscr{M}}\frac{1}{r}\frac{\partial}{\partial r}\omega^2r^2, \tag{15}$$

where

$$\Phi(\epsilon) = \epsilon(1-\epsilon)^2/\mu(\epsilon). \tag{16}$$

Since ω, $(\mathscr{E}^{-\frac{1}{2}}Hu)$ and $(\mathscr{E}^{-\frac{1}{2}}w)$ are explicitly given in table 1, (15) can be readily solved by the methods of characteristics.

In the non-rotating region I the solution is simply $\epsilon = \epsilon(0)$, i.e. no separation takes place. Table 1 shows that fluid from domain I is absorbed into the Ekman layers (at $z = 0^+, H^-$) and then effluxed into region III. Thus the important conjecture is that the volume fraction in the Ekman layers during spin-up is $\epsilon(0)$, whence the boundary conditions for (15) are

$$\epsilon(z = 0^+) = \epsilon(z = H^-) = \epsilon(0) \quad \text{for} \quad \mathrm{e}^{-\mathscr{M}\tau} \leqslant r \leqslant 1, \quad \tau > 0. \tag{17}$$

The behaviour of ϵ during spin-up is strongly governed by the parameter λ, the ratio of (developed) separation to spin-up timescales. If $\lambda < 1$ a considerable amount of separation takes place while rotation is established. For $\lambda \gg 1$, when spin-up is essentially completed the deviation from the initial $\epsilon(0)$ is still very small. Another critical parameter is the sign of α, as indicated in figures 2 and 3.

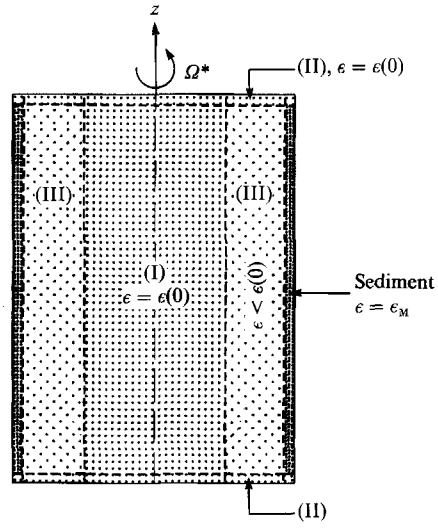

FIGURE 2. Qualitative volume fraction during spin-up of a mixture of heavy particles.

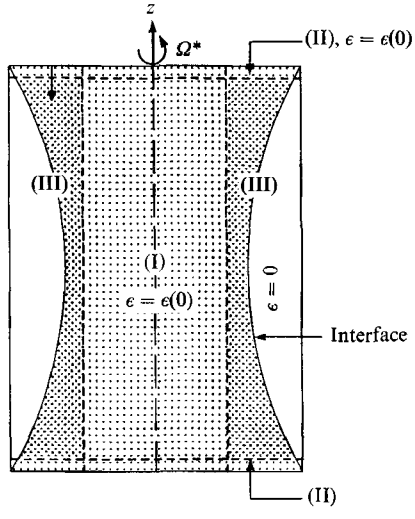

FIGURE 3. Qualitative volume fraction during spin-up of a mixture of light particles.

For heavier particles, $\alpha > 0$, in the rotating-mixture domain III, the normalized volume fraction $[\epsilon/\epsilon(0)]$ decreases with time, axial distance from the endplates (actually, from the Ekman layers) and radial distance from the spin-up front $r = e^{-\mathscr{M}\tau}$. The separated particles are expected to form a sediment on the outer wall, $r = 1$, of the container.

For lighter particles, $\alpha < 0$, in the rotating-mixture domain III, the normalized volume fraction $[\epsilon/\epsilon(0)]$ increases with time, axial distance from the endplates (actually, from the Ekman layers) and radial distance from the front $r = e^{-\mathscr{M}\tau}$. The particles migrate to the centre, leaving a region of pure fluid adjacent to the outer wall. The interface between the pure fluid and mixture has a peculiar shape, see figure 3, which is assumed to be a kinematic shock of zero thickness, coinciding with the

locus (r_p, z_p) of the particles effluxed by the Ekman layers at the rims $r = 1, z = 0^+$, H^-. Consider such a particle effluxed at τ_{init} at $z = 0^+$; its axial position at time $\tau_1 (> \tau_{init})$ is

$$z_p = \tfrac{1}{2}H\left[1 - \frac{1 - e^{-2.\mathscr{M}\tau_{init}}}{1 - e^{-2.\mathscr{M}\tau_1}}\right]; \tag{18}$$

and the corresponding radial coordinate is obtained by integrating

$$\frac{1}{\mathscr{M}}\frac{dx_p}{d\tau} = 2\frac{A}{1-A}x_p\left[1 - \frac{1}{x_p} - \frac{1}{\lambda\mathscr{M}}\frac{\Phi(\epsilon)/\epsilon}{A(1-A)}\left(1 - \frac{A}{x_p}\right)^2\right], \tag{19}$$

from τ_{init} to τ_1, subject to $x_p = 1$ at $\tau = \tau_{init}$, where $x_p = r_p^2, A = e^{-2.\mathscr{M}\tau}$.

In general, the integration of (19) is coupled to the solution of (16) by the presence of ϵ; for very small ϵ the 'dilute' approximation $\Phi(\epsilon)/\epsilon = 1$ simplifies the calculations. It is worth emphasizing that in the separation of a light-particle mixture starting from solid-body rotation the interface is expected to be cylindrical (Greenspan 1983), thus the shape of the interface becomes a stringent test of the relevance of the spin-up effects on separation.

These briefly mentioned asymptotic solutions have been used as guidelines and reference results for the numerical calculations. The latter also attempt to throw some light on uncertainties and difficulties that appear in the former approach. As opposed to the single-phase flow, little is presently known about the two-phase Ekman layers. Ungarish & Greenspan (1983) and Resnick (1991) studied the viscous flow induced by a rotating disk in a quiescent mixture, which is a good approximation to the shear flow on the endplates beneath the non-rotating core (region I). According to these investigations, the velocity field in the Ekman (here, rather von Kármán) layer is closely reproduced by the single-phase solution which accounts for the effective viscosity, and the volume fraction is that of the original mixture. However, in a sublayer of thickness $\beta^{\frac{1}{2}}E^{\frac{1}{2}}$ near the disk ϵ displayed a non-regular behaviour. The present numerical solutions did not encounter any difficulties that can be attributed to such a sublayer, and, in general, confirm the speculation that $\epsilon = \epsilon(0)$ in the Ekman layers.

Another problematic issue in the foregoing approximate solutions is the behaviour of ϵ and of the shock at the midplane $z = \frac{1}{2}H$. The pertinent trajectories start at the 'corner' $r = 1, \tau = 0, z = 0$ (or H) where the 'core' apparently has a non-physical behaviour. For this reason the theoretical approximations have been calculated and displayed only up to an interval of $0.05H$ from the midplane. Again, the numerical solution does not display any special features on and around the plane $z = \frac{1}{2}H$.

4. Numerical approach

The numerical computations are carried out in cylindrical coordinates in a rotating frame of reference. The velocity $\boldsymbol{v}$ used above is related to the velocity $\boldsymbol{u} = u\hat{\boldsymbol{r}} + v\hat{\boldsymbol{\theta}} + w\hat{\boldsymbol{z}}$ in the rotating frame by $\boldsymbol{v} = \boldsymbol{u} + \hat{\boldsymbol{z}} \times \boldsymbol{r}$. Cylindrical symmetry is assumed, so the unknowns u, v, w, p, ϵ are computed as functions of r, z, t. Given all flow-field variables at time level n, the momentum equation (2) and continuity equation (3) are first solved for velocity and pressure at time level $n+1$ using the volume fraction at time level n. The volume fraction is then advanced using the new velocity field.

As mentioned above, the original system (2)–(8) has been slightly simplified before the application of the numerical treatment. This simplification saves programming

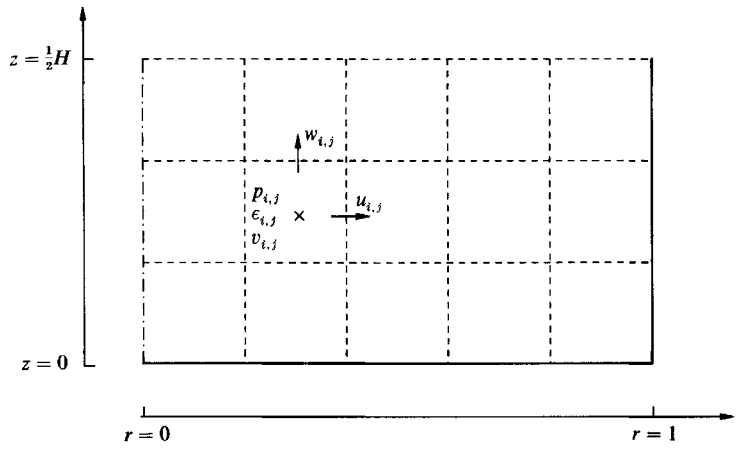

FIGURE 4. Grid cell used in the numerical computations.

and computational efforts but is not an essential part of the method. In the cases that will be studied here the parameter β and the product $\alpha\epsilon$ are small. In order to facilitate the numerical treatment described below, two small terms have been neglected in the equations above. Firstly, since (7) implies that $\boldsymbol{v}_{\mathrm{R}} = O(\alpha\beta)$, the last term on the right-hand side of the momentum equation (2) is seen to be of order $\alpha^2\beta^2\epsilon$. Secondly, when using the relation between $\boldsymbol{j}$ and $\boldsymbol{v}$ in (6) to replace $\boldsymbol{j}$ by $\boldsymbol{v}$ in the continuity equation (3), the resulting equation expressed in $\boldsymbol{v}$ is $\boldsymbol{\nabla}\cdot\boldsymbol{v} = O(\alpha^2\beta\epsilon)$. The right-hand side of this equation, as well as the term in the momentum equation mentioned above, are both small compared to retained terms and are neglected in the numerical treatment. Also, in (7), the acceleration on the right-hand side has been approximated by $r\omega^2\hat{\boldsymbol{r}}$, just as in the asymptotic theory in §3.

The numerical solution of the momentum and continuity equations follows the scheme presented by van Kan (1986). The spatial discretizations are done on a staggered grid of the standard type, see figure 4. The radial and axial velocities u, w are defined on cell boundaries, while azimuthal velocity v, pressure p and volume fraction ϵ are defined at cell centres. In the momentum equation, the convective term is discretized with an upwind formula used by Davis & Moore (1982). Second-order-accurate finite-difference discretizations are used for the remaining terms. In the present context the basic method for time stepping from $n(\mathrm{d}t)$ to $(n+1)(\mathrm{d}t)$ may be written as

$$(1+\epsilon^n\alpha)\left(\frac{\tilde{\boldsymbol{u}}-\boldsymbol{u}^n}{\mathrm{d}t}+\tfrac{1}{2}\boldsymbol{\nabla}(\boldsymbol{u}^n\cdot\boldsymbol{u}^n)+(\boldsymbol{\nabla}\times\boldsymbol{u}^n)\times\boldsymbol{u}^n+2\hat{\boldsymbol{z}}\times\tilde{\boldsymbol{u}}\right)$$
$$= -\boldsymbol{\nabla}p^n+E\boldsymbol{\nabla}\cdot(\mu(\epsilon^n)[\boldsymbol{\nabla}\tilde{\boldsymbol{u}}+(\boldsymbol{\nabla}\tilde{\boldsymbol{u}})^{\mathrm{T}}-\tfrac{2}{3}\boldsymbol{I}\boldsymbol{\nabla}\cdot\tilde{\boldsymbol{u}}])-\epsilon^n\alpha\hat{\boldsymbol{z}}\times(\hat{\boldsymbol{z}}\times\boldsymbol{r}), \quad (20)$$

$$\boldsymbol{\nabla}\cdot\left[\frac{\mathrm{d}t}{1+\epsilon^n\alpha}\frac{1}{2}\boldsymbol{\nabla}(p^{n+1}-p^n)\right] = \boldsymbol{\nabla}\cdot\tilde{\boldsymbol{u}}, \quad (21)$$

$$\boldsymbol{u}^{n+1} = \tilde{\boldsymbol{u}}-\frac{\mathrm{d}t}{1+\epsilon^n\alpha}\frac{1}{2}\boldsymbol{\nabla}(p^{n+1}-p^n). \quad (22)$$

Expression (20) is an equation for $\tilde{\boldsymbol{u}}$, which is solved by conjugate gradient iterations on the three different velocity components. Using this $\tilde{\boldsymbol{u}}$, the right-hand side of (21) may be computed, and the equation can be solved for the pressure increment from

time level n to $n+1$. This is also done by the conjugate gradient method. Finally the velocity field at the new time level is obtained from (22). Note that the original momentum equation is obtained by using (22) to replace $\tilde{\boldsymbol{u}}$ by $\boldsymbol{u}^{n+1}$ in the first term on the right-hand side of (22); $\tilde{\boldsymbol{u}}$ then still remains in the Coriolis and viscous terms. It is proved by van Kan (1986), for non-rotating incompressible flow, that $\tilde{\boldsymbol{u}} \approx \boldsymbol{u}^{n+1}$ (or more precisely $\tilde{\boldsymbol{u}} = \boldsymbol{u}^{n+1} + O(\mathrm{d}t^2)$). Then the appearance of $\tilde{\boldsymbol{u}}$ in the viscous and Coriolis terms means that these are treated implicitly, which is beneficial for the stability of the scheme. The theoretical proof is only for non-rotating flows, but we have tested the time-dependent accuracy for the rotating case with satisfactory results. The continuity equation is always satisfied by the new velocity field. This is seen by taking the divergence of (22) and noting that the divergence of the right-hand side is identically zero in virtue of (21).

After the new velocity field has been obtained, the new volume fraction field, ϵ^{n+1}, is calculated via the solution of (4). This is performed by the classical explicit MacCormack scheme, see Fletcher (1988). This method is quite accurate for hyperbolic problems, away from shocks where the dependent variable changes abruptly from one value to another. In the present problem such difficult regions are indeed present, namely the moving kinematic shock across which ϵ is expected to jump from 0 (in the pure fluid) to a value larger than $\epsilon(0)$ (in the mixture). At such locations, this scheme will give large non-physical oscillations. In order to remove these wiggles, and still have a sharp transition zone, an explicit artificial diffusive term has been added to the right-hand side of (4):

$$\frac{\partial \epsilon}{\partial t} + \nabla \cdot (\epsilon \boldsymbol{u}_{\mathrm{D}}) = \nabla \cdot \boldsymbol{F}. \tag{23}$$

Here $\boldsymbol{F} = (F, H)$ is the artificial diffusive flux. It is small whenever ϵ varies smoothly. The radial component of $\boldsymbol{F}$ at the outer boundary of cell i,j is

$$F_{ij} = K\,\mathrm{d}r^2 \left[(1-\eta) \left| \frac{\Phi'_{i+1,j} - \phi'_{ij}}{\epsilon_{i+1,j} - \epsilon_{ij}} \right| + \eta \left| \frac{\epsilon_{i+1,j} - \epsilon_{ij}}{\mathrm{d}r} \right| \right] \frac{\epsilon_{i+1,j} - \epsilon_{ij}}{\mathrm{d}r}, \tag{24}$$

where

$$\eta = \frac{\epsilon_{i+\frac{1}{2},j}}{\epsilon_{\mathrm{M}}}; \quad \Phi'_{ij} = \frac{\mathrm{d}}{\mathrm{d}\epsilon} \frac{\epsilon(1-\epsilon)^2}{\mu(\epsilon)} \bigg|_{\epsilon=\epsilon_{ij}}.$$

Here $\mathrm{d}r$ is the radial mesh spacing, K is a numerical parameter which is $O(1)$, typically a good choice is 0.3–0.7. The factor in square brackets, which may be regarded as the artificial diffusivity, consists of two terms which are weighted by η. At low volume fractions the first dominates and at volume fractions near ϵ_{M} the second dominates. The first term involves the function Φ' which in kinematic wave theory measures the velocity of wave propagation. It has been chosen in this manner to give a diffusivity that is proportional to the change in velocity of propagation on characteristics between mesh points. The second term in (24) reflects the absolute value of the gradient of ϵ, so that this contribution to the artificial diffusivity is small when ϵ varies smoothly. It was necessary to include this second term since it was found that the first gives too low diffusivities in regions with almost densely packed sediment, say in a range of $0.5 < \epsilon < \epsilon_{\mathrm{M}}$. A similar formula is used for the axial component of $\boldsymbol{F}$.

The present scheme is, evidently, of the 'shock capturing' (or 'smearing') type: the 'shock' appears in the global solution as a sharp but continuous transition zone. The alternative 'shock fitting' method treats the shock as a real discontinuity, using

explicitly the equation that specifies its motion; the solution is carried out separately in sub-regions demarcated by the shock, and matched by 'jump' conditions. The latter method is expected to yield more accurate solutions, but its formulation, discretization, programming and computation require considerably larger investments than the former. Although some research on the implementation of 'shock fitting' schemes to multidimensional flow of suspensions is of interest, the 'shock capturing' method seems preferable, just as in the more mature branch of computational compressible aerodynamics. Moreover, the present investigation indicates that finite-difference solvers for single-phase flows can be extended to tackle suspensions via the incorporation of some new terms in the existing balances and the addition of (23). With a 'shock fitting' approach the upgrading of a single-phase scheme to a suspension flow solver is not so straightforward and must rely on a deeper understanding of the expected flow field and 'jump' conditions between pure fluid, mixture and sediment domains.

The stability of the total scheme is governed by the CFL criterion since convective terms have been treated by an explicit upstream difference formula (Davis & Moore 1982), and Coriolis and viscous terms are implicit. In practice this means that the time step $\mathrm{d}t$ should satisfy $\mathrm{d}t \leqslant 0.3/\max(u/\mathrm{d}r, w/\mathrm{d}z)$. Note that this is the stability requirement that is obtained in a similar treatment of single-phase flow. Thus, existing single-phase codes may be practically extended to mixture flow by adding the equation for the volume fraction. In these respects the numerical solution of the 'mixture' model is superior to the 'two-fluid' model whose discretization and use for a similar geometry was presented by Ungarish (1988, 1990), namely: (*a*) the stability of the latter is also restricted by the drag terms which, in the present scaling, yields $\mathrm{d}t < \beta$; (*b*) the two-fluid formulation cannot be treated as an extension of single-phase flow.

Meshes with at least 50 axial points and 60–120 radial points were used. As soon as the Ekman layers are resolved, the essential effect of increasing the resolution is to sharpen numerical shocks. Outside the shock regions, the solution did not change when the radial resolution was increased from 60 to 120 points.

This code has been also used for other rotating sedimentation problems such as spin-up from rest of a mixture of heavy particles, slow sedimentation in a mixture that rotates rigidly and sedimentation in an axial channel with axial throughflow.

The code was run on an Alliant FX2800 computer with 16 processors, which has a peak performance of 40 MFlops/processor. No great effort was made to parallelize the code, and it was mostly run on a single processor. A typical execution time for the simulation of 6.28 non-dimensional time units, i.e. one revolution of the container, on a 60×50 grid was 300 s CPU.

5. Results

5.1. *Two flow fields with* $E = 10^{-4}, \lambda = 1$, *different* $\epsilon(0)$

The two flow fields considered here have in common the following parameters: aspect ratio $H = 0.5$, Ekman number $E = 10^{-4}$, particle Taylor number $\beta = 4 \times 10^{-2}$, reduced density difference $\alpha = -0.5$. The initial volume fraction, $\epsilon(0)$, is 10% in the first case and only 1% in the second. The corresponding enhancement of shear effects, represented by $\mathscr{M}$ of (12), are 1.15 and 1.01.

In both cases the ratio of separation to spin-up timescales, $\lambda = E^{\frac{1}{2}}/|\alpha|\beta H$, equals 1 and the solution was carried out up to $\tau = 2.5$ (i.e. $t = 125$, see (13), which corresponds to about 20 revolutions of the container).

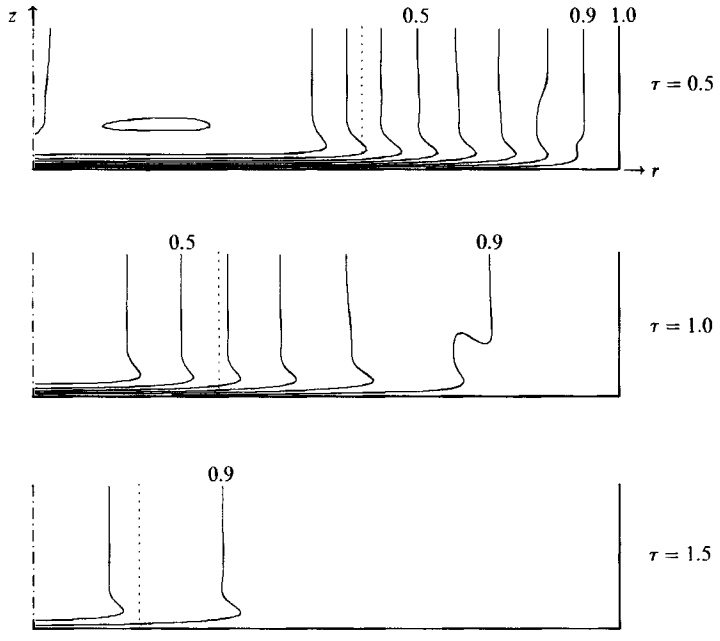

FIGURE 5. Contours of constant ω for $\epsilon(0) = 0.1$, various τ. The levels are $0.1, \ldots (0.1)$. The dotted line shows the asymptotical spin-up 'front'.

Owing to symmetry about the midplane only the domain

$$0 \leqslant z/H \leqslant 0.5 \ (0 \leqslant z \leqslant 0.25)$$

is detailed. The Ekman (or von Kármán) layer on the plate is expected to occupy the subregion $z/H < 3E^{\frac{1}{2}}/H = 0.06$, about $\frac{1}{8}$ of the axial extent of the flow field. The number of grid points used in the numerical simulation was 120×50 in the radial and axial directions, respectively. Hence about six axial (non-stretched) mesh intervals are encompassed by the Ekman layer, so that a good resolution of this shear region is anticipated.

Figures 5–7 refer to the case $\epsilon(0) = 0.1$. Figure 5 shows the angular velocity of the mixture at $\tau = 0.5$, 1.0, 1.5. The theoretical predictions are essentially confirmed. A shear layer appears on the plate. At $\tau = 0.5$ a non-rotating region is seen inside $r \approx 0.5$, in plausible agreement with the spin-up front which separates the rotating and non-rotating regions III and I in the approximate solution. The spin-up front is 'smeared' by viscous effects, a behaviour known from the single-phase analysis (Venezian 1970; Hyun *et al.* 1983) which, however, has not been incorporated in the asymptotic analysis discussed in §3. At $\tau = 1$ the non-rotating core has almost disappeared, and the mixture is approaching a state of solid-body rotation. At $\tau = 1.5$, spin-up is fairly complete: ω has reached at least 90% of its final value for about 90% of the fluid contained in the cylinder. The calculated ω displays a dependency on the axial coordinate; this interesting discrepancy with the asymptotic results is caused by the presence of the dispersed phase and will be discussed later.

Figure 6 shows contours of constant volume fraction at $\tau = 0.5$, 1.0, 1.5, 2.0, 2.5. Since α is negative, particles are lighter than the fluid and settle towards the centre. The complicated field of ϵ, varying with time, radius and axial distance from the plate is evident. As predicted by the analytical solution, a region of clear fluid develops near the outer wall. Adjacent to the pure fluid domain there is a region of

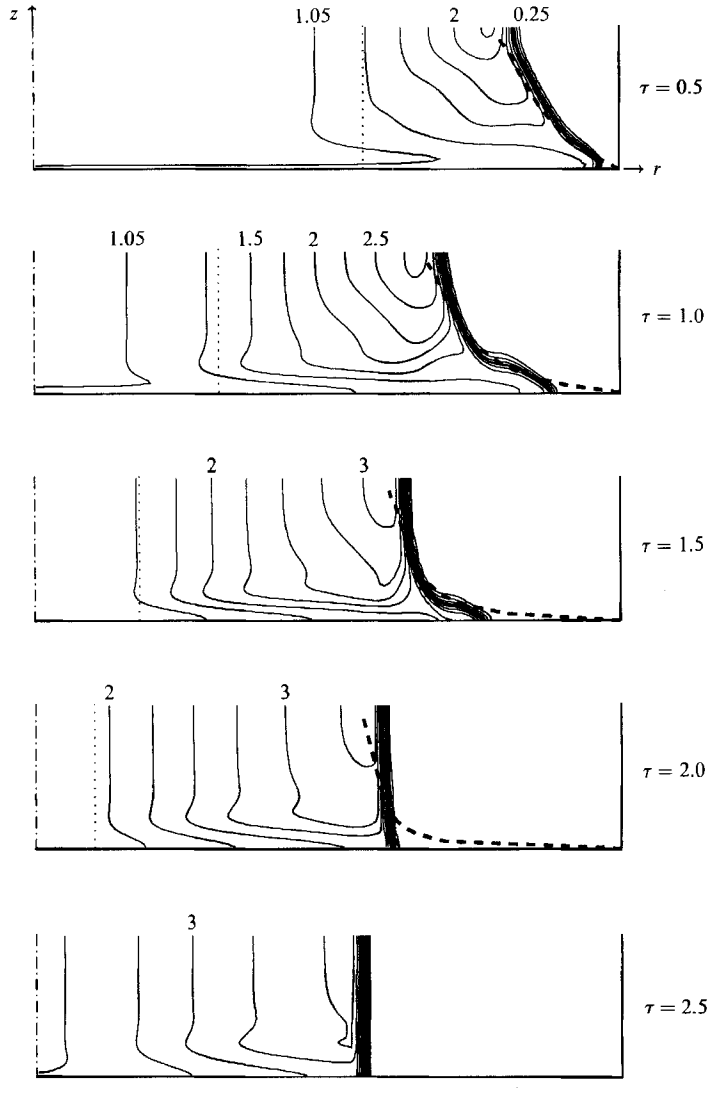

FIGURE 6. Contours of constant $\epsilon/\epsilon(0)$ for $\epsilon(0) = 0.1$, various τ. The levels are 0.25, 0.50, 0.75, 0.95, 1.05, 1.25, ... (0.25). Also shown: the asymptotical spin-up 'front' (dotted line) and kinematic shock (heavy dashed line).

increased particle volume fraction, $\epsilon/\epsilon(0) > 1$. The transition zone is sharp: typically, $\epsilon/\epsilon(0)$ changes by a factor of 10 over a dimensionless distance of 0.05. The $\epsilon/\epsilon(0) > 1$ region extends inward, a little beyond the position of the theoretical spin-up front. In the region occupied by the non-rotating core there is no centrifugal force, consequently no separation has taken place, and the volume fraction is unchanged. At $\tau = 1.0$, when the non-rotating core has almost vanished, the concentrated region extends further inward and the maximum concentration has increased. The interface separating the clear fluid from the mixture has travelled further inward. At $\tau = 1.5$, the concentrated region extends all the way to the centre. The interface is becoming more cylindrical and does not reach the rim. At $\tau = 2.0$ and 2.5, the fluid is practically in solid-body rotation, but at this time the mixture is fairly separated: the pure fluid region occupies more than 60% of the container. This confirms the

conclusion that when λ is not large a considerable amount of separation occurs before the mixture achieves a state of solid-body rotation. For $\tau > 2$ the mixture core continues to shrink and the volume fraction to increase towards a state of maximum packing $\epsilon = \epsilon_M$; this is a slow process because of the strong hindering effect of the close-packed particles.

Superimposed on the numerically calculated contours are the locii of the interface between mixture and clear fluid predicted by the asymptotic approach, as explained in §3. The agreement is good from both qualitative and quantitative aspects. In the finite-differences computation the interface has been 'captured' via the calculation of ϵ, hence it has a finite thickness of at least three mesh intervals. The asymptotic approach assumes that this interface is an infinitesimally thin kinematic shock.

The theoretical interface is (asymptotically) attached at the rim where the endplate meets the cylindrical wall. The reason for this is that the radial flow in the Ekman layer on the endplate that is induced during spin-up carries fresh mixture of the initial concentration from the non-rotating core to the rim along the endplates. The asymptotic theory argues that the flow in the Ekman layers during spin-up is rapid enough to bring the mixture to the rim before any separation has occurred. This argument also led to the prediction that $\epsilon = \epsilon(0)$ in this shear layer. The numerically computed interfaces are however seen to be attached to the endplate at a finite distance from the rim; moreover, the radius of attachment moves inward during the process. This is because: (*a*) the parameter $|\alpha|\beta$, considered infinitesimally small in the analytical approximations, has the value of 0.02 in the present runs; (*b*) the intensity of the flow in the Ekman layers decays like $(1-\omega)$, i.e. with both τ and r, see table 1; owing to these factors, the tendency of the lighter particles to move inwards will overcome, at some finite distance from the rim, the drifting velocity of the radial motion in the shear layer. More details are presented in the Appendix.

The volume fraction in the Ekman layers, which was conjectured by the asymptotic theory to be $\epsilon(0)$, is indeed seen to be only slightly raised at $\tau = 0.5$ and 1.0. At later times ϵ also increases in the boundary layer. The reason for this is the same as above, i.e. that the settling velocity becomes comparable to the radial boundary-layer transport as the radial flow in the Ekman layer decays.

It was mentioned that the theoretical treatment of the interface becomes problematic as z/H approaches 0.5. Figure 6 indicates that this is not a serious deficiency since the numerical solution does not contain any dramatic behaviour near the midplane that has not been captured by the asymptotic theory. (On the contrary, it is possible that the approximate analytical solution hints at a delicate effect that is beyond the resolution of the finite-difference code used here.)

The dependency of ω in the core on the axial coordinate z, as observed in figure 5, turns out to be caused by the variations of ϵ in the axial direction. In particular, at $\tau = 1$, the curves of constant ω are not parallel to the z-axis around $r \approx 0.6$ where ϵ increases significantly with z. The interpretation is as follows. The axial momentum equation indicates that when the Ekman number is small there is no mechanism to support axial variations of the pressure, consequently during the spin-up we anticipate $p = p(r, \tau)$. At the same time, the main force balance in the radial direction is between the radial pressure gradient, $\partial p(r,\tau)/\partial r$, and the centrifugal term $(1+\epsilon\alpha)\,\omega^2 r$. Hence the latter product must be independent of z, and since ϵ varies with z, this variation has to be compensated for by a variation in ω. Essentially, the effect is similar to the more familiar 'thermal wind' result, i.e. an axial variation in the fluid's density causes an opposite axial change in angular velocity; the increase of temperature is parallel to an increase in volume fraction here because both reduce the

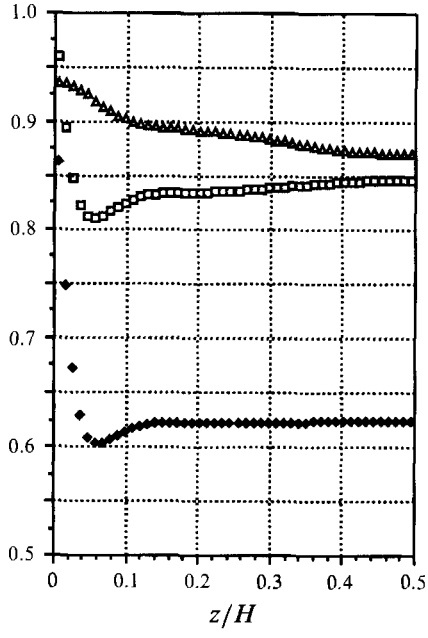

FIGURE 7. Plot of non-dimensional density $(1+\epsilon\alpha)$ ($\triangle$), ω ($\square$) and $(1+\epsilon\alpha)\omega^2 r$ ($\blacklozenge$) *vs.* z, at $\tau = 1.0, r = 0.595$.

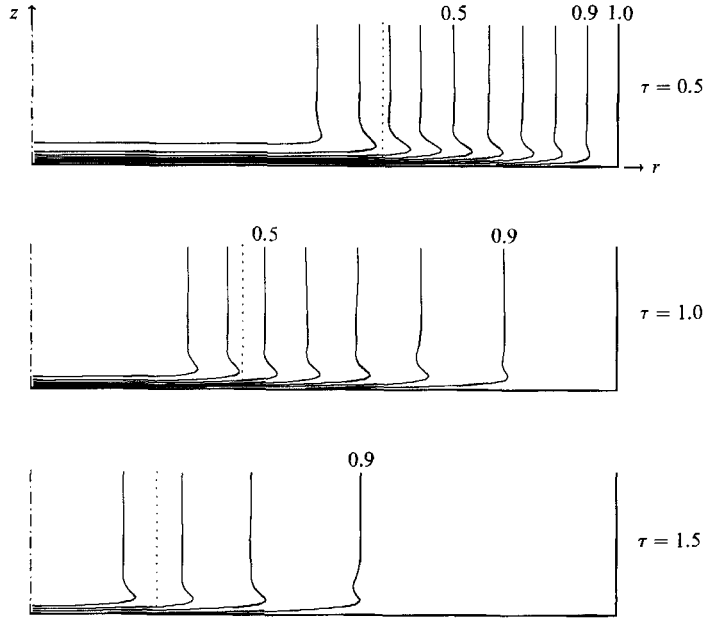

FIGURE 8. Contours of constant ω for $\epsilon(0) = 0.01$, various τ. The levels are $0.1, \ldots (0.1)$. The dotted line shows the asymptotical spin-up 'front'.

local density of the rotating fluid. This interpretation is verified in figure 7. This graph shows, at $\tau = 1.0$ and $r = 0.595$, the total non-dimensional density $(1+\epsilon\alpha)$, angular velocity ω and $(1+\epsilon\alpha)\omega^2 r$ as functions of z. There is a clear dependence on z of both density and angular velocity, but the product $(1+\epsilon\alpha)\omega^2 r$ is constant outside

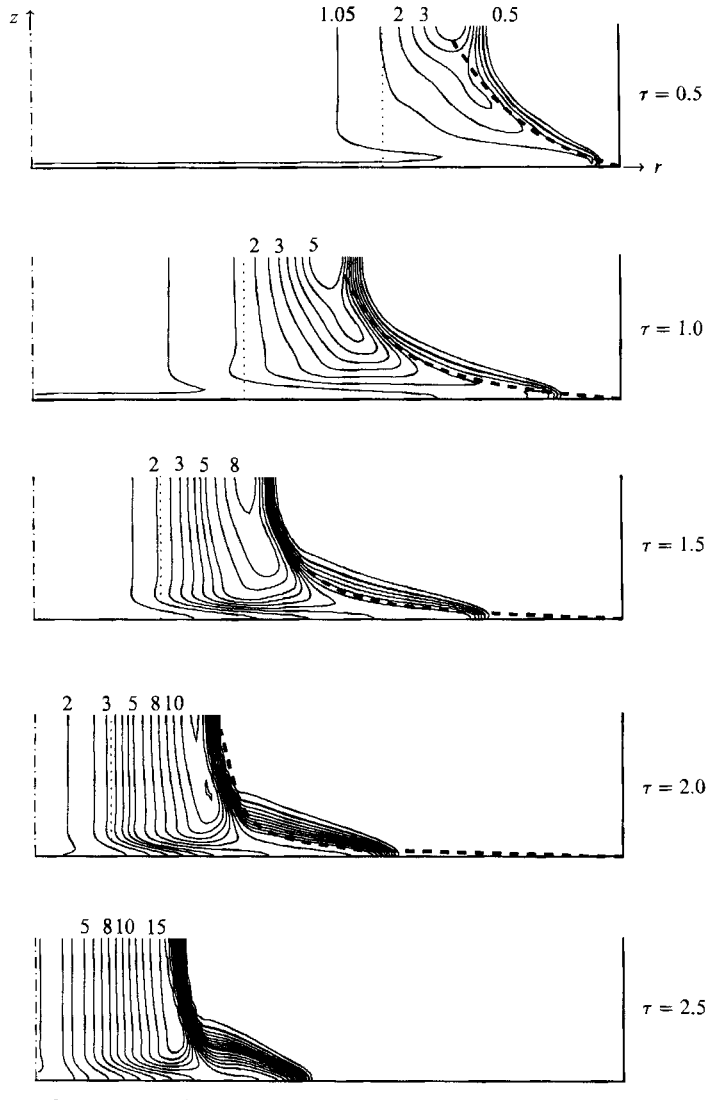

FIGURE 9. Contours of constant $\epsilon/\epsilon(0)$ for $\epsilon(0) = 0.01$, various τ. The levels are 0.5, 0.95, 1.05; 1.5–5.0 (0.5); 6.0, ... (1.0). Also shows the asymptotical spin-up 'front' (dotted line) and kinematic shock (heavy dashed line).

the Ekman layer, as expected. The asymptotic theory did not account for this effect due to the assumption that $\epsilon\alpha$ is a negligibly small quantity. The fact that the 'jump' of ϵ across the kinematic shock causes a 'jump' in ω implies that an inclined detached shear layer of Ekman type exists around this interface to smooth out the velocity discontinuity. The structure of this interface becomes therefore more complex than anticipated, an interesting topic for further investigation. It is noted in passing that ω in figure 7 displays a clear maximum at $z \approx 0.025$; the theoretical linear Ekman layer predicts such a maximum at $z = \frac{3}{4}\pi\mathscr{E}^{\frac{1}{2}} = 0.027$.

Figures 8 and 9 are similar to figures 5 and 6 but for the case with the initial volume fraction $\epsilon(0) = 0.01$ instead of 0.1. This means that there will be less variation of viscosity and settling velocity, cf. (7), (8), and also that the variation in absolute density is small so that the dynamical effects that caused ω to depend on z in the

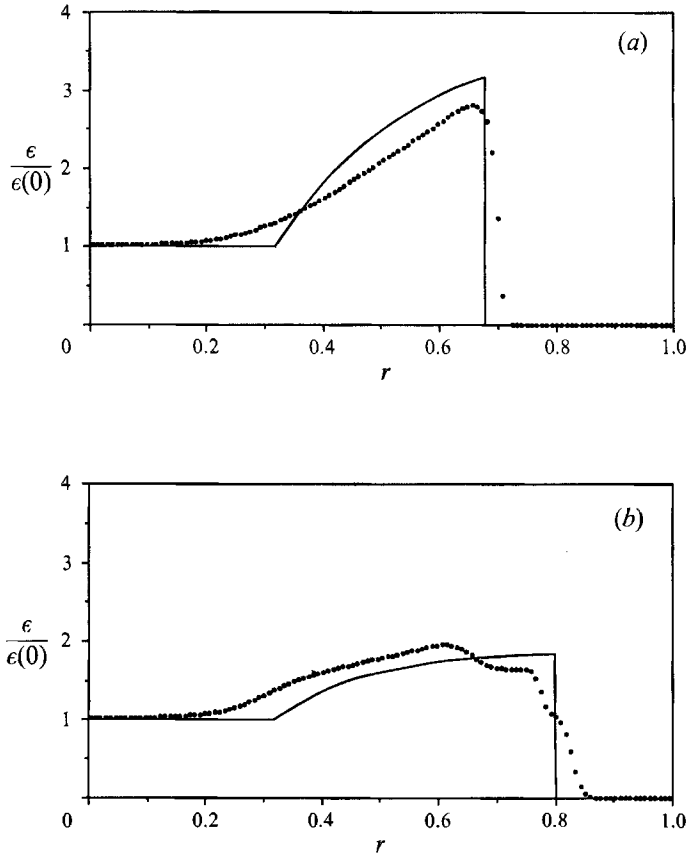

FIGURE 10. Profiles $\epsilon/\epsilon(0)$ *vs.* r for $\epsilon(0) = 0.1$, at $\tau = 1$, at (*a*) $z/H = 0.45$, (*b*) $z/H = 0.1$: ——, asymptotic theory; ●, numerical results.

interior are weak (in this sense, the run is closer to the range of validity of the asymptotic theory).

Figure 9 shows contours of constant $\epsilon/\epsilon(0)$. There are some noticeable differences compared to the $\epsilon(0) = 0.1$ case in figure 6. Evidently, settling proceeds faster in the $\epsilon(0) = 0.01$ case, the clear-fluid interface advances further in, and the relative increase in volume fraction in the concentrated region is larger. This is due to the hindering effect, which becomes less pronounced at smaller volume fraction. The hindering coefficient for the particle settling velocity, $[1-\epsilon(0)]^2/\mu[\epsilon(0)]$, equals 0.62 for $\epsilon = 0.1$ and 0.96 for $\epsilon = 0.01$. On the other hand, the spin-up is slightly slower for the $\epsilon = 0.01$ case, which is due to the smaller effective viscosity (recall the appropriate values of the coefficient $\mathscr{M}$). In fact, the velocity field is almost exactly the same as in single-phase spin-up. The numerical contour lines of ϵ are again superimposed on the interfaces predicted by the analytical approximations. The agreement is good. The radial positions of the attachment of the interface to the Ekman layer are quite similar to those of the previous run at corresponding τ, in accordance with the estimates of the Appendix.

For a more stringent comparison, profiles of ϵ versus r from the numerical computations were plotted together with the asymptotic predictions. Figure 10 shows ϵ as function of r for the case with $\epsilon(0) = 0.1$, at $\tau = 1.0$, at two axial positions: near the midplane and closer to the 'edge' of the Ekman layer. It is seen that the

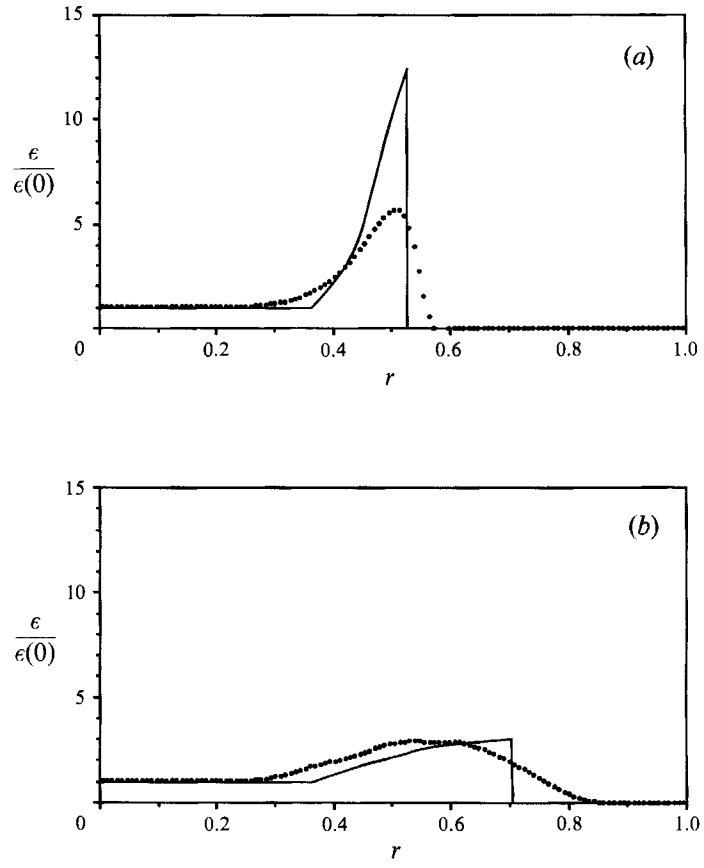

FIGURE 11. As figure 10 but for $\epsilon(0) = 0.01$.

numerically computed shocks are fairly sharp, and that their location agrees reasonably well with the analytical predictions. The transition from non-separated to separating mixture is smoother in the numerical profiles, because the spin-up front that separates regions I and III, figure 1, is actually smoothed by viscosity, as previously mentioned.

In figure 11 the corresponding profiles for the $\epsilon(0) = 0.01$ case are shown. Here it is seen that the finite-difference code is less successful in reproducing the shocks than in the $\epsilon = 0.1$ case. However, the jump in $\epsilon/\epsilon(0)$ is now larger, which probably enhances the contribution of the artificial diffusivity term, (24). Moreover, at $z/H = 0.1$ the 'shock' is very inclined, see figure 9; hence the sharp variation of ϵ is in the axial direction rather than in the radial one, which yields an apparent wider 'smearing' in the profile *vs.* r.

5.2. *Flow field with* $E = 1.01 \times 10^{-5}, \lambda = 0.68$

The code was used to compute a configuration that has been studied in a laboratory test described by Ungarish (1991). The relevant parameters are: aspect ratio $H = 2.094$, Ekman number $E = 1.01 \times 10^{-5}$, relative density difference $\alpha = -0.034$, particle Taylor number $\beta = 0.0648$ and initial particle volume fraction $\epsilon(0) = 0.01$. The ratio of settling time to spin-up time λ was 0.68; settling is thus slightly faster than spin-up. This combination of parameters is closer to the asymptotical requirements than the previously discussed case owing to the smaller E and α. (Also,

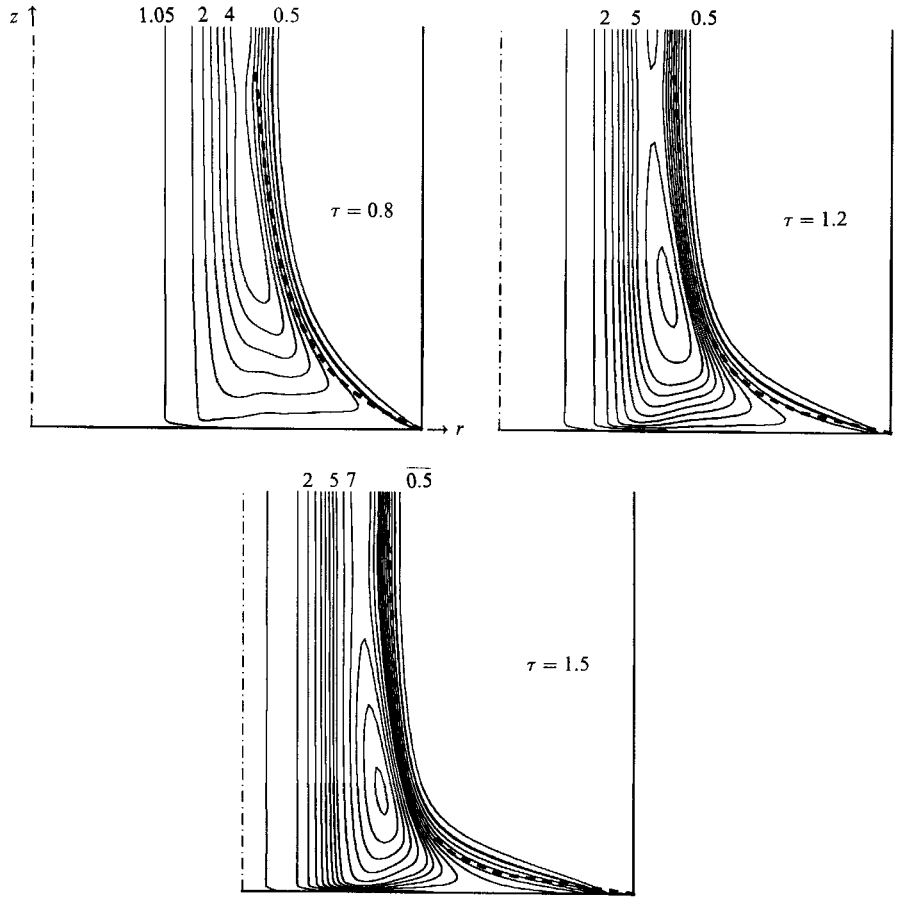

FIGURE 12. Contours of constant $\epsilon/\epsilon(0)$ for the experimental case, various τ. The levels are 0.5, 0.95, 1.05; 1.5–5.0 (0.5); 6.0, ... (1.0). Also shown is the asymptotic kinematic shock (heavy dashed line).

the aspect ratio is 2.094 instead of 0.5, which makes the ratio of Ekman-layer thickness to height even more favourable.) On the other hand, the difficulty of numerical resolution increases. Here simulations were carried out up to $\tau = 1.5$, corresponding to $t = 988$, i.e. approximately 160 revolutions. A grid with 200 axial and 100 radial points was used.

In figure 12 volume fraction fields at $\tau = 0.8$, 1.2, 1.5 are shown. Again, owing to symmetry about the midplane only the portion $0 \leqslant z/H \leqslant 0.5$ is detailed. The qualitative picture is similar to that seen above: a non-rotating core with $\epsilon = \epsilon(0)$ inside a region with increased volume fraction. At the outer wall there is a pure-fluid region. The most apparent difference here is that the interface is attached closer to the rim; this is because $|\alpha|\beta$, to which the displacement from the rim is proportional, see (A 2) in the Appendix, is now ten times smaller than in the previous runs. Superimposed on these graphs are the interface shapes that are predicted by the asymptotic theory. The agreement is excellent.

Figure 13 displays photos of the experiment performed by Ungarish (1991) at the same values of τ as computed for figure 12. The qualitative agreement in the shape of the interface is striking. Unfortunately it is not feasible to extract reliable quantitative information from these photos but they certainly provide good support for the results presented in this paper.

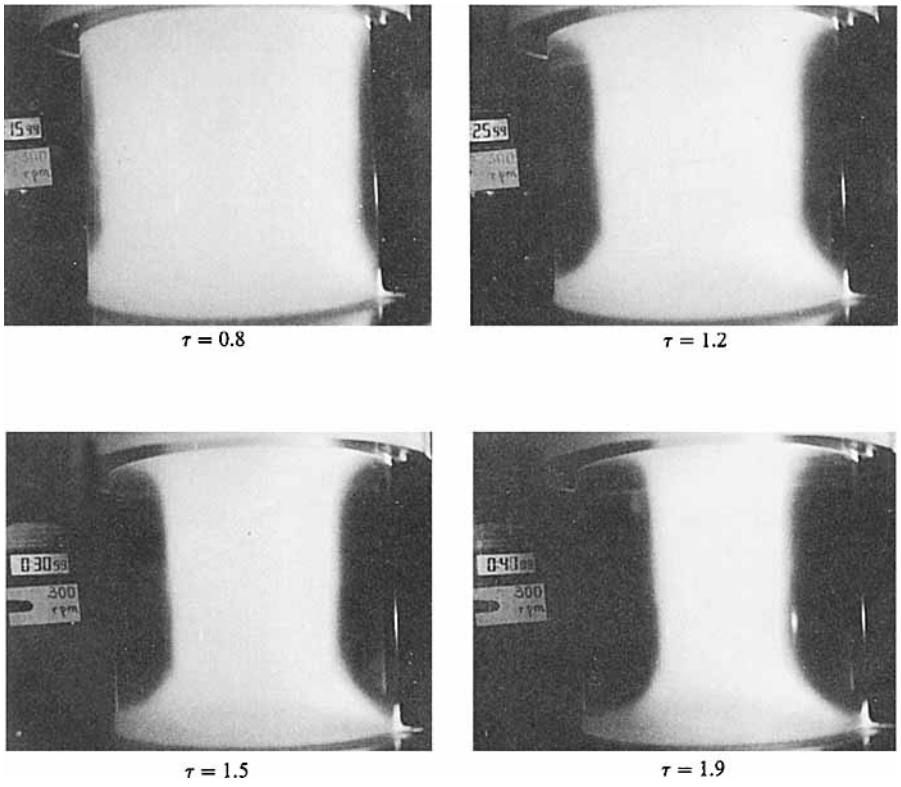

FIGURE 13. Photographs from experimental tests.

6. Concluding remarks

The velocity and volume fraction (concentration) fields, during spin-up from rest of a separating suspension of light particles in fluid, were simulated by a finite-differences version of the (slightly simplified) mixture-averaged equations of motion. Artificial diffusion was incorporated to facilitate numerical 'shock capturing' treatment of the expected kinematic discontinuities. Qualitative and quantitative comparisons with asymptotic theory were emphasized.

It was found that reasonable numerical solutions could be obtained for this rather complex flow, and that the kinematic shock representing the interface between clear fluid and mixture could be reproduced sharply. The resolution of this interface deteriorates when the volume fraction is small (in our case, 1 %), a topic that requires further investigations and improvement. The simulations are quite CPU time consuming because the large number of points and time steps needed due to resolution and stability considerations. Efforts for parallelization are necessary to improve the performances.

In the cases considered it was shown that at 1 % initial volume fraction of particles (with $|\alpha| = |\rho_D - \rho_C|/\rho_C = 0.5$) the velocity field is affected only very slightly by the presence of particles, and is very close to that in spin-up of a single-phase fluid. However, at 10 % volume fraction the flow field differs significantly from the single-phase solution. Among other things, the axial variation of volume fraction causes an axial variation of the azimuthal velocity in the interior, which is impossible in a single-phase flow.

In general the agreement between the asymptotic theory and the simulations is

	r_a	
τ	Eq. (A 2)	figures 6, 9
0.5	0.96	0.96
1.0	0.86	0.88
1.5	0.67	0.77
2.0	0.45	0.60

TABLE 2

excellent. Although the asymptotic theory breaks down on the axial midplane, the simulations do not show any dramatic behaviour there and the agreement between the approximate results and simulation close to the midplane is still satisfactory. The discrepancies – which are larger for cases with Ekman numbers that are not very low, at larger times and at higher volume fraction – can all be consistently explained by the deviations from the assumptions employed by the asymptotic theory. Also, the axial mesh interval used here was sufficiently small to reproduce the Ekman layers but too coarse for detecting the one-particle sublayer predicted by previous investigations. This did not cause any observable deficiencies in the computations. The good agreement between the numerical and the asymptotic solutions gives considerable confidence in both approaches and provides encouragement for applying similar methods in even more complicated situations. The hope is that experimental progress will follow soon.

The research of M.U. was supported by the Fund for the Promotion of Research at the Technion.

Appendix. Attachment radius estimates

It is argued that the kinematic shock is attached to the endplate at the farthest radial positions where particles are carried by the Ekman layer, denoted subsequently as r_a. In other words, r_a is the radial position where, in the Ekman layer adjacent to region III, $\max(u_D) = 0$.

According to (6)

$$u_D = \boldsymbol{j}\cdot\hat{\boldsymbol{r}} + (1-\epsilon)\,u_R.$$

Since in this layer $u_R \approx -|\alpha|\,\beta([1-\epsilon(0)]/\mu[\epsilon(0)])\,r$ (see (7)) and $(\boldsymbol{j}\cdot\hat{\boldsymbol{r}})_{\max} \approx 0.3(1-\omega)\,r$ (from the theory of rotating single-phase fluids), the radius of interest, r_a will be given by

$$u_D \approx \{0.3[1-\omega(r_a,\tau)] - |\alpha|\,\beta[1-\epsilon(0)]^2/\mu[\epsilon(0)]\}\,r_a = 0. \tag{A 1}$$

Substituting $\omega(r,\tau)$ from table 1 and rearranging yields

$$\frac{1}{r_a^2} = 1 + 3.3(e^{2.4\tau}-1)\,|\alpha|\,\beta\frac{[1-\epsilon(0)]^2}{\mu[\epsilon(0)]}. \tag{A 2}$$

For the run of §5.1 one obtains the results shown in table 2 (the results for $\epsilon(0) = 0.1$ and 0.01 are very close so we do not distinguish between the cases in table 2).

The approximation (A 2) apparently captures the leading mechanism that governs the position of attachment of the interface to the endplate. The discrepancies are probably caused by numerical smearing.

REFERENCES

DAVIS, R. W. & MOORE, E. F. 1982 A numerical study of vortex shedding from rectangles. *J. Fluid Mech.* **116**, 475–506.

FLETCHER, C. A. J. 1988 *Computational Fluid Mechanics.* Springer.

GREENSPAN, H. P. 1983 On centrifugal separation of a mixture. *J. Fluid Mech.* **127**, 91–101.

HYUN, J. M., LESLIE, F., FOWLIS, W. W. & WARN-VARNAS, A. 1983 Numerical solutions for spin-up from rest in a cylinder. *J. Fluid Mech.* **127**, 263–281.

ISHII, M. 1975 *Thermo-Fluid Dynamic Theory of Two-phase Fluids.* Eyrolles.

ISHII, M. & ZUBER, N. 1979 Drag coefficient and relative velocity in bubbly, droplet or particle flows. *AIChE J.* **25**, 843–854.

KAN, J. VAN 1986 A second order accurate pressure-correction scheme for viscous incompressible flow. *SIAM J. Sci. Comput.* **7**, 870–891.

RESNICK, R. I. 1991 Numerical analysis of two-phase rotating flows. M.Sc. thesis, Technion – Israel Institute of Technology, Haifa, Israel.

UNGARISH, M. 1988 Numerical investigation of two-phase rotating flow. *Intl J. Multiphase Flow* **14**, 729–747.

UNGARISH, M. 1990 Spin-up from rest of a mixture. *Phys. Fluids* A**2**, 160–166.

UNGARISH, M. 1991 Spin-up from rest of a light-particle suspension in a cylinder: theory and observations. *Intl J. Multiphase Flow* **17**, 131–143.

UNGARISH, M. & GREENSPAN, H. P. 1983 On two-phase flow in a rotating boundary layer. *Stud. Appl. Maths* **69**, 145–175.

VENEZIAN, G. 1970 Nonlinear spin-up. *Top. Ocean Engng* **2**, 87–96.

WEDEMEYER, E. H. 1964 The unsteady flow within a spinning cylinder. *J. Fluid Mech.* **20**, 383–399.